Available online at www.sciencedirect.com
ScienceDirect
Trans. Nonferrous Met. Soc. China 31(2021) 3643−3658
Transactions of Nonferrous Metals Society of China
www.tnmsc.cn

Theoretical and experimental studies on fabrication of two-layer aluminum−copper pipe by friction stir additive manufacturing

Mehdi FALAHATI NAQIBI[1], Majid ELYASI[1], Hamed JAMSHIDI AVAL[2], Mohammad Javad MIRNIA[1]

1. Department of Mechanical Engineering, Babol Noshirvani University of Technology, Shariati Avenue, Babol 47148-71167, Iran;
2. Department of Materials Engineering, Babol Noshirvani University of Technology, Shariati Avenue, Babol 47148-71167, Iran

Received 3 December 2020; accepted 29 June 2021

Abstract: Using a friction stir additive manufacturing (FSAM) process, the fabrication of a two-layer aluminum−copper pipe was studied experimentally and numerically. For this purpose, by presenting a 3D thermo-mechanical model in ABAQUS software, the temperature and strain distributions during the process were studied. The simulation results show that, although the rotational-to-traverse speed ratio with a good approximation can predict the heat input during welding, it is not a precise measure to predict the occurrence of defects in the weld cross-section. There is a good agreement between the predicted and experimental thermal results, and the maximum relative error is 4.1% in estimating the maximum temperature during welding. Due to heat and severe plastic deformation in the stir zone, the aluminum−copper intermetallic compounds ($CuAl_2$ and Cu_9Al_4) are formed. The maximum hardness in the stir zone is 301.4 $HV_{0.1}$ in sample welded with an overlap of −0.5 mm. The ultimate tensile strength and elongation of the two-layer pipe fabricated by friction stir additive manufacturing are (319.52±2.31) MPa and 19.47%, respectively.
Key words: friction stir welding; thermo-mechanical simulation; two-layer Al−Cu pipes; microstructure; mechanical properties

1 Introduction

Additive manufacturing (AM) refers to one of the fabrication methods in which the final product is fabricated by adding a source of materials based on the desired geometry [1,2]. The AM method is different from manufacturing methods involving reduction methods such as machining in which the material is mechanically removed from the original large-sized billet, casting and forging in which the main mold or shaft is used to create the desired geometric shape, and joining in which product is created from the connection of arbitrary subsets. The fundamental difference between the traditional and additive construction methods has led to a number of new techniques [2]. One of the AM methods, which has attracted special attention of researchers, is the friction stir additive manufacturing (FSAM) method. In one of the most common FSAM methods, the two sheets are connected to each other using friction stir welding process and lap joining design. Due to the application of heat and plastic deformation during the process, the connection of two sheets occurs at interface. In the field of fabrication of two- or multi-layer sheet composites using the FSAM process, several reports have been presented by various researchers [3−8].

The use of bimetallic pipes in order to resist corrosion on the inner surface and the strength and low cost of the outer surface metal have been

Corresponding author: Majid ELYASI, E-mail: elyasi@nit.ac.ir, elyasima@yahoo.com
DOI: 10.1016/S1003-6326(21)65754-0

considered. In many cases, the inner and outer surfaces of pipes are exposed to different environments and therefore require different properties. The production of bimetallic pipes in different methods including: extrusion [9,10], multi-billet extrusion [11], explosive welding [12,13], diffusion bonding [14], centrifugal casting [15] and spin bonding [16], hydraulic expansion and thermal hydraulic adaptation [17] and magnetic pulse method [18] has been reported in various sources. Many of these methods face technological, metallurgical and economic limitations. Cost-effective production and at the same time the quality of the joining are the key points in the production of double-layer pipes. One of the processes that can achieve these two goals at the same time and can be implemented in different diameters and thicknesses of pipes, is the friction stir welding (FSW) process. Important parameters in the production of bilayer pipes by FSW are the tool plunge depth, the ratio of rotational to traverse speed of the tool and also the overlap of different passes that affect the formation of unwanted intermetallic compounds and ultimately the mechanical properties of the joint. The joint strength in the FSW of dissimilar materials is much higher than that of other joining processes due to the metallurgical and mechanical natures of the created bond [19−21]. Therefore, cylindrical bimetallic parts can be welded first in the form of initial cross-section and after the production of bimetallic pipe, this sample can be formed into the final bimetallic part by means of forming processes such as hydroforming. In the field of FSW of circular sections, limited studies have been carried out by researchers [22−27]. Studies on FSW of circular sections in lap joining design are as follows. JAMSHIDI and FALAHATI [28] investigated the lap FSW process of AA5083-H321 aluminum pipe with a diameter of 360 mm to AA5083-O aluminum pipe with a diameter of 350 mm. In this study, the effect of tool rotational speed and pipe rotational speed in the FSW process was investigated by tensile test and metallographically examination. Finally, the rotational speeds of 650 and 800 r/min and the traverse speed of 40 mm/min were introduced as the best parameters for welding in their study. LI et al [29] investigated the production of two-layer aluminum−copper pipe by friction welding process. Although they have successfully produced two-layer aluminum−copper pipes by friction welding process, the main problem of their procedure is the impossibility of performing the process in producing pipes with long lengths and large diameters. TAVASSOLIMANESH and ALAVI [30] investigated the FSW of aluminum and copper pipes as a lap joint scheme. They examined only one weld line on the tube and did not examine the effect of joining parameters such as the overlap of different passes.

With the development of hardware as well as mathematical models, it is possible to use simulation methods to study thermo-mechanical evolutions during the FSW. In the field of simulation of FSW process on circular sections there are studies by IQBAL et al [31] and LAMMLEIN et al [32]. Using a viscoplastic model, IQBAL et al [31] studied the temperature distribution and material flow in the FSW of AA6005 aluminum alloy. They showed that a tool plunge depth of 0.3 mm led to finer grain size in the stir zone as well as flawless joint. LAMMLEIN et al [32] investigated the butt-welding process of a 6-mm AA6061-T6 aluminum pipe by experimental and numerical methods. They evaluated FSW process using a computational fluid dynamics (CFD) model. This model was used to simulate and predict the temperature distribution and the flow of materials. The simulation results regarding the axial force applied in the welding process with the information obtained from the experimental process show the accuracy of the modeling.

According to the available sources, the experimental and numerical study of the fabrication process of two-layer pipes using the FSAM process and the study of process parameters have not been done. Due to the importance of the subject, in this research the construction of two-layer AA5086 aluminum/C12200 copper pipe using FSAM process was studied experimentally and numerically. For this purpose, by presenting a three-dimensional thermo-mechanical model, the temperature and strain distributions during the process were studied. Then, using numerical results, microstructural changes and mechanical properties of two-layer AA5086 aluminum/C12200 copper pipe were investigated.

2 Mathematical model

Due to the large plastic deformation in the FSW process, a method must be used to correctly predict the heat generation and plastic strains. For this purpose, three approaches can be used: Lagrangian, arbitrary Lagrangian−Eulerian (ALE) and couple Euler and Lagrangian (CEL) methods [33]. If the Lagrangian approach is used, due to the deformation of the elements and the displacement of nodes, there will be excessive distortion in the elements, which leads to inefficient analysis, unless much finer elements are used throughout the model, which will increase the cost and time of analysis. The ALE method uses a procedure in which the nodes are still movable, but the shape of the elements is approximately preserved during the plastic deformation and changes only in terms of dimensional scale. Although this method is capable of simulating the FSW, the analysis time will be very long and it will be possible for the analytics to stop at any stage of the simulation. In the present study, CEL technique has been used for simulation. In this technique, the coupling of Eulerian and Lagrangian elements is used. Unlike the Lagrangian element, Eulerian elements do not experience any change in their geometry, and the geometry of these elements will remain constant throughout the simulation. The Eulerian element is initially empty of the material and the material must be attributed to it in the desired volume. Due to these properties, Eulerian elements are simply able to model large deformations and have a higher efficiency in terms of simulation cost [33,34].

In the present study, using the ABAQUS finite element software with the CEL approach, the dissimilar welding process of AA5086 aluminum and C12200 copper pipe is simulated. A coupled thermo-mechanical model is used to analyze the mechanical and thermal responses during FSW. During FSW, due to heat generation by friction and plastic deformation, the properties of the material change. Therefore, by using coupled thermo-mechanical model it is possible to consider thermal and mechanical responses simultaneously. By using general equilibrium equation, it is possible to predict the mechanical response during FSW:

$$\rho a+F_{\mathrm{b}}=\mathrm{div}(\sigma) \tag{1}$$

where ρ, σ, F_{b}, and a are density, stress, body force, and acceleration, respectively.

The stress created in the FSWed sample is due to the elastic and plastic deformation, and the thermal history. The general stress equation that represents stress and strain relationship is as follows:

$$S=\boldsymbol{M}(\varepsilon^{\mathrm{e}}+\varepsilon^{\mathrm{p}}+\varepsilon^{\mathrm{t}}) \tag{2}$$

where S is the shear stress, $\boldsymbol{M}$ is the stress matrix, and ε^{e}, ε^{p} and ε^{t} represent elastic, plastic and thermal strains, respectively. The equation governing transient heat transfer in the system can be expressed as follows:

$$\rho c_p\frac{\partial T}{\partial t}=\frac{\partial}{\partial x}\left[k\frac{\partial T}{\partial x}\right]+\frac{\partial}{\partial y}\left[k\frac{\partial T}{\partial y}\right]+\frac{\partial}{\partial z}\left[k\frac{\partial T}{\partial z}\right]+\eta S\dot{\varepsilon}_{\mathrm{pl}} \tag{3}$$

where c_p is the specific heat capacity of material, T is the temperature, k is the thermal conductivity, η is the plastic deformation energy efficiency, and $\dot{\varepsilon}_{\mathrm{pl}}$ is the plastic strain rate tensor. The boundary conditions at the tool/workpiece interface are considered as follows:

$$k\frac{\partial T}{\partial \boldsymbol{n}}\bigg|_{\text{pin and shoulder}}=q_{\mathrm{surf}} \tag{4}$$

where $\boldsymbol{n}$ is the unit outward normal vector, and q_{surf} represents the heat generated in the interface of the tool and the workpiece. The q_{surf} can be considered as follows:

$$q_{\mathrm{surf}}=\mu p\dot{\gamma} \tag{5}$$

The heat generated at the interface of the tool and the workpiece is dependent on the coefficient of friction (μ), the normal pressure (p), and the slip rate ($\dot{\gamma}$). The convection heat transfer mechanism with a heat transfer coefficient of 20 W/(m^2·°C) is considered on free contact surface of tool and workpieces. An effective convection heat transfer coefficient of 1000 W/(m^2·°C) is considered on the other contact surfaces (lower surface of the copper pipe and the upper surface of the tool). The initial temperature of the workpiece and tool is assumed to be 20 °C. 2556 and 89745 C3D4T (four nodes with degree of freedom of temperature and displacement) elements are considered in the tool and pipes, respectively. Tangential motion in contact conditions related to the interface of surfaces is considered in the present model using Coulomb's law of friction. The thermo-physical properties and the elastic modulus used in the

simulation are reported in Table 1 [35−39]. Also, for the mechanical properties and flow stress of the material at different temperatures and strain rates, the data presented in Ref. [40] have been used.

3 Experimental

AA5086 aluminum alloy pipes and C12200 copper have been used. The chemical compositions of the two alloys are listed in Table 2. The outer pipe in this study is aluminum AA5086 with the diameter, length and thickness of 44.2, 150 and 1.5 mm, respectively. The copper pipe is also considered to be the inner pipe with the diameter, length and thickness of 41.2, 150 and 1.38 mm, respectively. In order to perform FSW on the pipe and to stabilize the workpiece properly for welding, the setup designed according to Fig. 1 has been used. The tool's rotational speed is powered by an 8.085 kW engine and gearbox. Two rotary gearboxes and torque boosters were used to rotate the workpiece, along with a 2.205 kW engine. The rotational speed variations of the workpiece were determined by inverter. Also, the milling machine table was used for linear movement of the tool parallel to the rotational motion of the workpiece. The cruise control of the machine was controlled by a gearbox called the forward gearbox. FSW was performed by a cylindrical pin with pin and shoulder diameters of 3 and 10 mm, respectively. Pin length of 2 mm, tool tilt angle of 3°, and plunge depth of 0.2 mm were considered. The welding parameters as reported in Table 3 are the overlap of different passes, rotational and traverse speeds of the tool. Henceforth, the samples are named in the form of rotational speed–traverse speed–welding overlap. The overlap of the passes is named based on the distance of the outer surface of the pin in different passes. For example, in the overlaps of 0 and +0.5 mm, the outer surface of the pin is tangent and +0.5 mm apart to each other, respectively, in two passes. In order to compare the thermal results obtained from the simulation and experimental measurements and to verify the simulation results, the temperature during welding was measured by a k-type thermocouple with a diameter of 1 mm. Figure 2 shows the location of the thermocouple on the cross-section of the pipes.

After welding, the specimens were cut perpendicularly to the welding direction to study

Table 1 Thermo-physical properties and elastic modulus of materials [35−39]

Material	Density/ ($kg·m^{-3}$)	T_α/°C	α/ (10^{-6} °C^{-1})	T_k/°C	k/ ($W·m^{-1}·°C^{-1}$)	T_{c_p}/°C	c_p/ ($J·g^{-1}·°C^{-1}$)	T_E/°C	Elastic modulus, E/GPa
AA5086	2657	25	23.8	25	127	25	0.900	25	70 .0
		200	25.5	250	151	250	0.960	100	67.8
		300	26.8	300	154	300	0.980	200	60.7
		400	28.9	400	158	400	1.020	300	51.0
		500	31.5	500	169	500	1.113	400	37.4
C12200	940	20	16.8	20	398	20	0.385	20	120
		127	17.6	136	386	100	0.393	100	117
		227	18.3	246	377	200	0.403	200	113
		327	18.9	323	374	300	0.412	300	105
		427	19.5	414	367	400	0.420	400	98
		527	20.2	476	358	500	0.424	500	94
		627	20.8	561	351	600	0.430	600	81

T_α, T_k, T_{c_p}, and T_E are temperatures related to α, k, c_p, and E, respectively

Table 2 Chemical compositions of AA5086 aluminum alloy and C12200 copper

Alloy	Al	Ti	Zn	Cr	Mg	Mn	Cu	Fe	Si	P
AA5086	Bal.	0.15	0.25	0.25	4.5	0.7	0.1	0.5	0.4	–
C12200	–	–	–	–	–	–	Bal.	–	–	0.04

Table 3 Friction stir welding parameters and levels

Parameter	Level
Rotational speed, ω/(r·min^{-1})	400, 500, 600, 700
Traverse speed, v_x/(mm·min^{-1})	40, 60, 80
Overlap of FSW passes/mm	−0.5, 0, +0.5

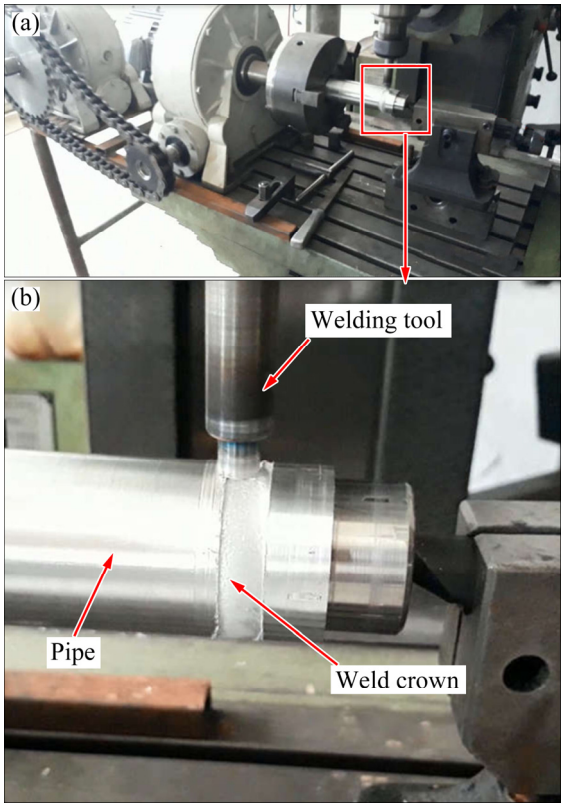

Fig. 1 Setup for fabricating two-layer tube by friction stir welding

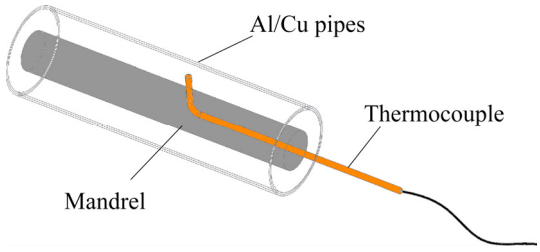

Fig. 2 Schematic view of temperature measurement during processing

the microstructure. After grinding and polishing, the modified Poulton's solution containing two separate solutions (25 mL of nitric acid, and 1 g of chromic acid dissolved in 12 mL of water; 12 mL of hydrochloric acid, 6 mL of nitric acid, 1 mL of fluoric acid and 1 mL of water) was used for etching AA5086 alloy and 50 mL HNO_3 solution and 50 mL H_2O were used to etch copper. A more detailed study of microstructural changes was performed by scanning electron microscopy (SEM). The mechanical properties of the welded samples were measured using ring hoop tension test (RHTT) and microhardness measurement. In order to measure the microhardness on the joint cross-section, the applied force was 100 g and the test time was 15 s. The RHTT was performed according to procedure reported in Ref. [41].

4 Results and discussion

4.1 Effect of rotational and traverse speeds on thermo-mechanical behavior

Firstly, welding was performed using welding pass overlap of 0 at rotational speed in the range of 400−700 r/min and traverse speed in the range of 40−80 mm/min. According to preliminary studies, the welded specimens with a rotational speed of 600 r/min and traverse speeds of 40 and 60 mm/min were without defects. The general results of the weld cross-section visual inspection are shown in Fig. 3. The defects observed in the samples were in the form of cavities or tunnel defects. It is difficult to state the exact cause of the defect formation in the welded samples, but it is possible to justify the defect in the samples welded by FSW process based on the heat input and material flow under FSW tool [42−44]. Based on Refs. [45−47], if the ratio of rotational speed to traverse speed of the tool is assumed as a criterion of heat input per unit length of weld, defects will be observed in welded samples with speed ratio of less than 10 r/min and more than 15 r/mm.

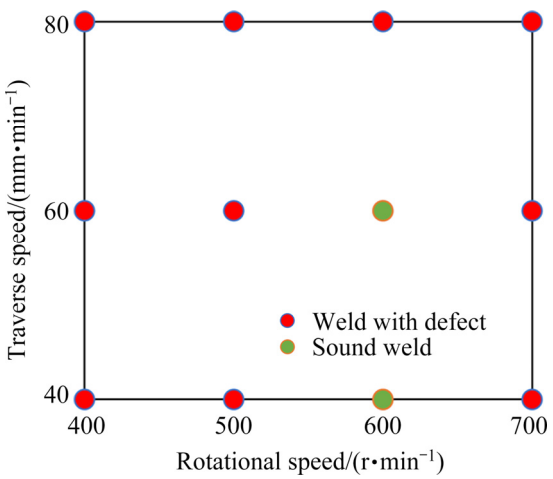

Fig. 3 Welding process window and corresponding weld defects

The cross-sections of the specimens with the minimum and maximum speed ratios along with the cross-section of the sound welds are shown in Fig. 4. At low heat input, as the tool moves forward, during material flow from advancing side to retreating side, the material temperature drops before it flows back to the advancing side, so there will not be enough material on the advancing side to fill the hole created by pin. The predicted temperature on the advancing side in the sample welded with rotational and traverse speeds of 400 r/min and 40 mm/min, respectively, shows that the maximum temperature in the stir zone is 445 °C while in the sample welded with rotational and traverse speeds of 600 r/min and 40 mm/min, respectively the maximum temperature at the same position is 495 °C. This can confirm the accuracy of the above justification for the occurrence of defect in low heat input conditions. However, the occurrence of defects at high speed ratio, despite the high heat input, is due to the excessive turbulent flow of materials in the stir zone [48−50]. Under these conditions, a suitable flow of material is not provided to fill the cavity on the advancing side. It can be seen that in welds performed with rotational speed of 500 r/min and traverse speed of 40 mm/min, rotational speed of 400 r/min and traverse speed of 40 mm/min, and rotational speed of 700 r/min and traverse speed of 60 mm/min, although the speed ratio is in the range of 10−15 r/mm, a tunnel defect has been observed in the weld. This shows that although the heat input can be used as a criterion for quality control of welding, the important point is that this criterion does not take into account the effect of plastic strain and its effect on material flow [51]. In other words, it can be said that at rotational speeds of 400 and 500 r/min, the improper flow of material and also at a rotational speed of 700 r/min due to turbulent flow may have led to defects in the stir zone. This observation shows that the use of numerical models that consider the effects of strain and heat simultaneously can be effective in controlling the properties and characteristics of the weld.

The results for the temperature profile obtained by simulation in Sample 600-40-0 are shown in Fig. 5. It is noteworthy that the temperature profile near the tool is asymmetric, so that on the advancing side the maximum temperature is higher than that on the retreating side. This is due to the asymmetric nature of the friction stir welding process, which causes a difference in plastic strain between the two sides. Of course, it should be noted that this temperature difference is small due to the presence of copper in the substrate because copper loses most of the heat due to its high heat sink capability. The welding temperature profile is controlled by the heat generation rate of the heat source on the workpiece and the welding heat loss rate. It can be seen that the temperature profile is more concentrated in the front part of the tool due to heat transfer with the

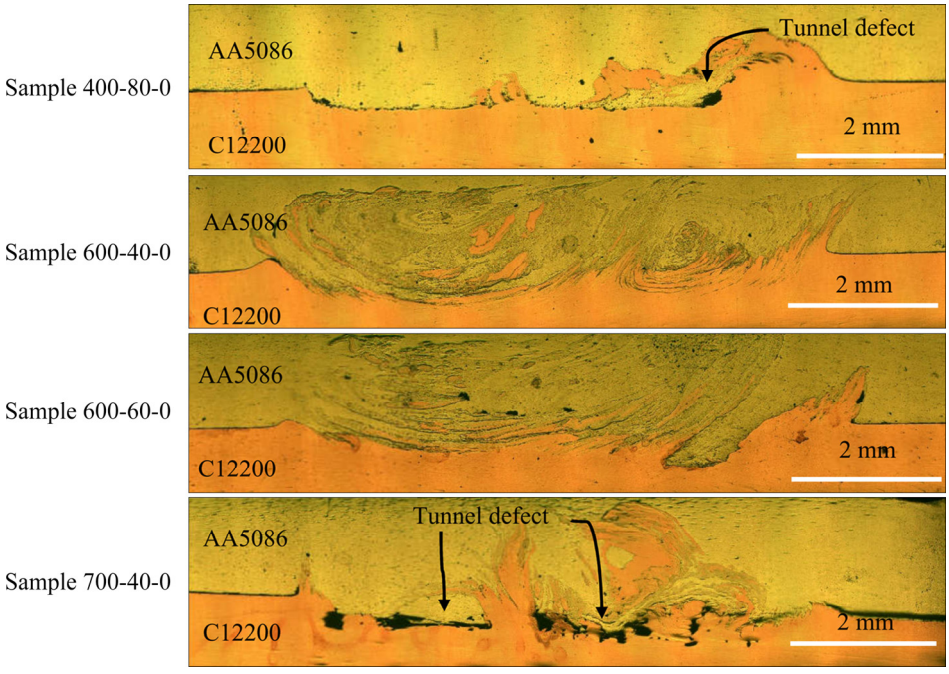

Fig. 4 Cross-sections of welded specimens

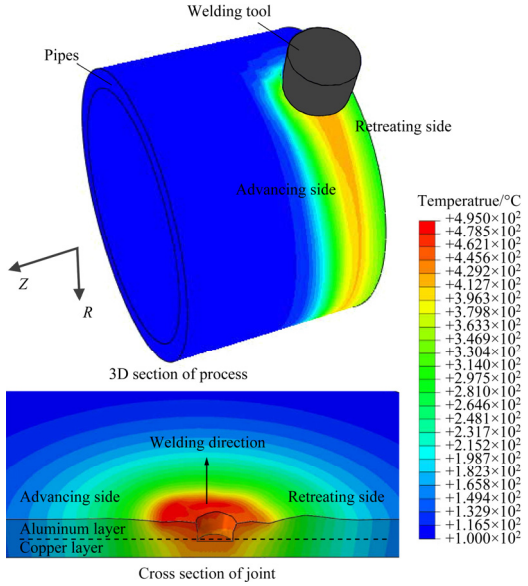

Fig. 5 Predicted temperature field for Sample 600-40-0

cooler workpiece and in the back part of the tool the temperature profile is wider due to the effect of lower temperature gradient made by welded zone.

The heat generated during the process is obtained through the friction between the tool/workpiece and the plastic deformation. The total heat produced and the contribution of heat generated by plastic deformation and frictional work predicted from simulation are reported in Table 4. As can be seen, the role of frictional heat in the total heat generation is far greater than the effect of heat due to plastic deformation. The high slip rate on the contact surfaces as a result of the tool rotation speed and the force exerted by the tool can lead to this high contribution of frictional work in total heat generation [52]. Although the contribution of heat due to plastic deformation is small, not considering this amount of heat means ignoring 8%−13% of the total heat, which in total can have a negative effect on the accuracy of the model results. According to Table 4, it can be seen that at a constant rotational speed, with increasing the traverse speed, the total heat generation decreases. It should be noted that this reduction is due to the reduction in both heat generated through friction and plastic deformation. The reduction in heat generation is the result of reduced contact time between the workpiece and the tool at a particular point.

Another important point that emerges from the results is the increase in the contribution of heat produced through plastic deformation relative to the heat produced through friction by increasing the traverse speed at a constant rotational speed. For example, in Sample 600-40-0 the contribution of heat due to plastic work is 8.55%, while in Sample 600-80-0 the contribution of heat due to plastic work is 10.70%. It is also observed that although by decreasing the ratio of traverse-to-rotational speed, the total heat per unit length of weld (ratio of total heat to traverse speed) increases at a constant rotational speed, by changing the rotational speed this ratio is not the exact criterion of welding heat input. In other words, it can be said that the

Table 4 Summary of energy dissipation during welding process

Sample No.	Energy dissipation of friction/kJ	Contribution of friction/%	Energy dissipation of plastic deformation/kJ	Contribution of plastic deformation/%	Total energy dissipation/kJ
400-40-0	18.47	91.53	1.71	8.47	20.18
500-40-0	24.15	91.65	2.20	8.35	26.35
600-40-0	25.78	91.45	2.41	8.55	28.19
700-40-0	26.85	91.11	2.62	8.89	29.47
400-60-0	16.19	89.99	1.80	10.01	17.99
500-60-0	19.20	89.30	2.30	10.70	21.50
600-60-0	22.45	90.19	2.44	9.81	24.89
700-60-0	25.11	90.45	2.65	9.55	27.76
400-80-0	15.53	89.05	1.91	10.95	17.44
500-80-0	17.43	87.89	2.40	12.11	19.83
600-80-0	21.03	89.30	2.52	10.70	23.55
700-80-0	23.20	89.54	2.71	10.46	25.91

simultaneous effect of friction and plastic deformation determines the amount of heat per unit length of weld. Figure 6 compares the maximum temperature in the stir zone obtained through simulation and experimental measurements in terms of rotational-to-traverse speed ratio. It is observed that although there is no linear trend between the ratio of rotational-to-traverse speed and the maximum temperature of the stir zone, with a good approximation it can be stated that by increasing this ratio the maximum temperature of stir zone increases.

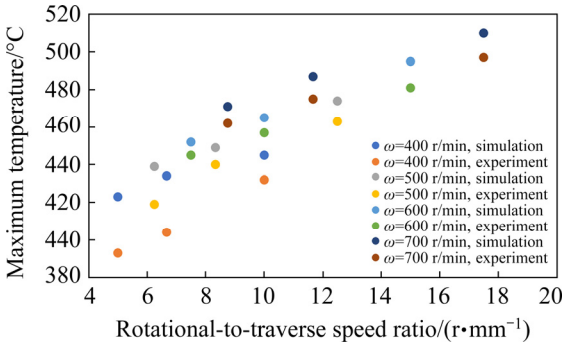

Fig. 6 Relationship between rotational-to-traverse speed ratio and maximum temperature in stir zone

Figure 7 shows the strain rate profile perpendicular to the welding direction obtained by simulation for Sample 600-40-0. It is observed that the strain rate on the welding section is not symmetric and the strain rate on the advancing side is slightly higher than that on the retreating side. This is due to the higher speed gradient on the advancing side. It is also observed that by moving in the thickness direction of the workpiece, the deformed zone decreases and the place where the maximum strain rate occurs is closer to the contact surface of the pin and the workpiece. According to similar results reported by other researchers [53], this is due to the sharp reduction in velocity in the thickness direction at distances beyond the contact surface of the workpiece with the pin.

4.2 Effect of overlap of different passes

4.2.1 Influence on thermo-mechanical behavior

After determining the appropriate rotational and traverse speeds, the weld fracture load was determined by performing shear tensile test on Samples 600-40-0 and 600-60-0. The maximum fracture forces for Samples 600-40-0 and 600-60-0

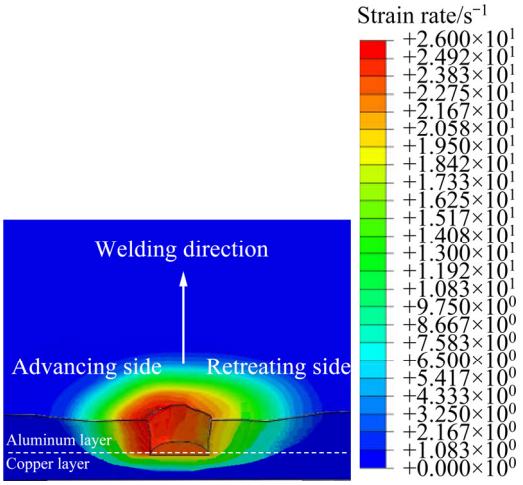

Fig. 7 Predicted strain rate distribution for Sample 600-40-0

were 3.4 and 2.9 kN, respectively. According to the maximum fracture force for Sample 600-40-0, the effect of overlapping of different passes at a rotational speed of 600 r/min and a traverse speed of 40 mm/min was investigated. Figure 8 shows the cross-sections of the welded specimens with different overlaps. As can be seen in all three overlaps, the weld cross-section is sound. If we consider the size and distribution of copper particles in the stir zone as a criterion of the uniformity of the stir zone, it can be seen that with increasing overlap or decreasing the overlap of passes compared to zero overlap, the copper particle size in the stir zone increases and the uniformity of the particles distribution is reduced.

Using the results obtained from process simulation as well as experimental temperature measurements, the effect of the overlap of different passes on the maximum temperature and also the maximum plastic strain during the welding process is compared in Fig. 9. It is observed that with the increase of the overlap of different passes, the maximum temperature obtained during the process has increased. This result can also be seen in the simulation and experimental measurement results. Although in the simulation results this difference is less than that in the experimental results, the increase in temperature with increasing overlap of different passes can be related to two issues. Firstly, due to the overlap of passes, the heat from the first pass acts as preheating of the second pass, as a result, as the overlap of the passes increases, the temperature increases. The next point is that in the

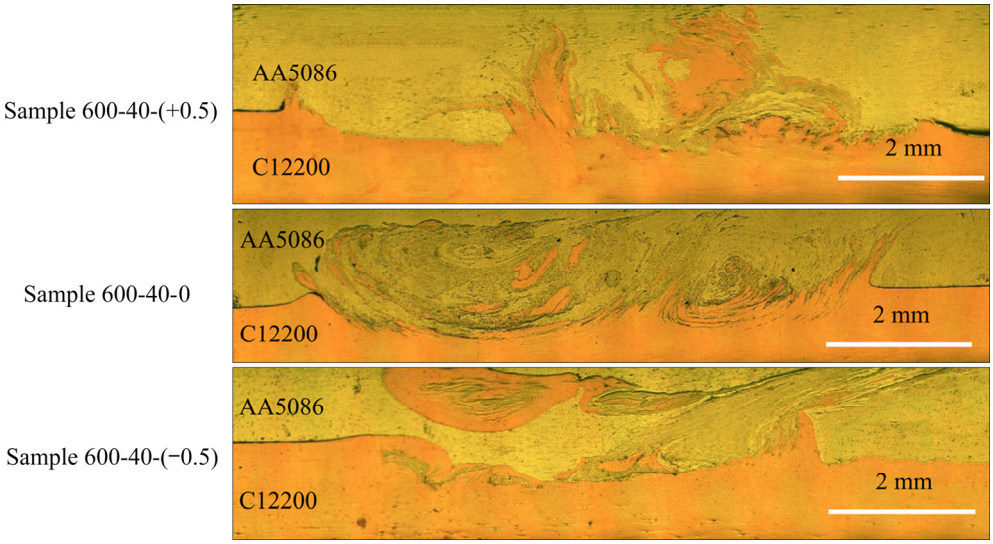

Fig. 8 Cross-sections of welded specimens with different overlaps

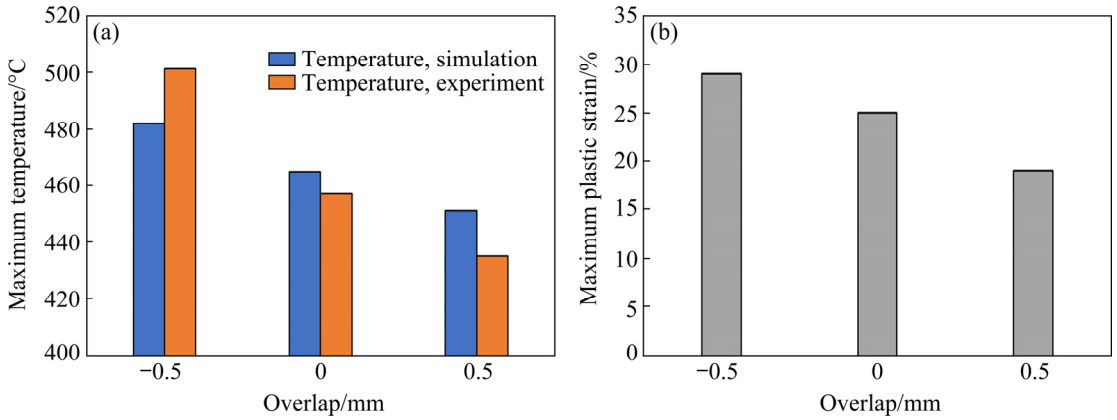

Fig. 9 Effect of overlap on maximum temperature (a) and maximum plastic strain (b) during welding process

first pass in the stir zone a composite of copper, aluminum and Al−Cu intermetallic is formed, and as a result, due to the formation of composite and intermetallic compounds, stir zone made in the first pass shows more resistance to deformation, which will increase the heat caused by friction and deformation. Of course, it should be noted that in the simulation of the second pass, the properties of the material were considered to be the same as those in the simulation of the first pass, probably the lower temperature in the simulation results could be due to the consideration of these conditions. It is also observed that with the increase of overlap, due to the increase of temperature, the plastic strain will increase.

4.2.2 Influence on mechanical properties

The results of microhardness test in samples welded with different overlaps are shown in Fig. 10. The hardness was measured at a distance of 0.5 mm parallel to the joint interface on both sides of the copper and aluminum alloys. The results of the hardness test showed that the maximum hardness in the stir zone was in sample welded with overlap of −0.5 mm and equal to 301.4 $HV_{0.1}$. In all specimens the hardness of the stir zone on the aluminum alloy side increased compared to the aluminum base metal. The decrease in grain size in the stir zone due to the dynamic recrystallization and the formation of equiaxed fine grains is one of the reasons for the increase in the hardness in the stir zone on the aluminum alloy side. On the other hand, the detachment of copper particles and their dispersion in the stir zone as well as the formation of the aluminum−copper intermetallic compound are the factors affecting the increase of hardness in the stir zone [54]. Although the hardness differences on both sides of the aluminum alloy are observed in the stir zone in all three overlaps, by increasing the

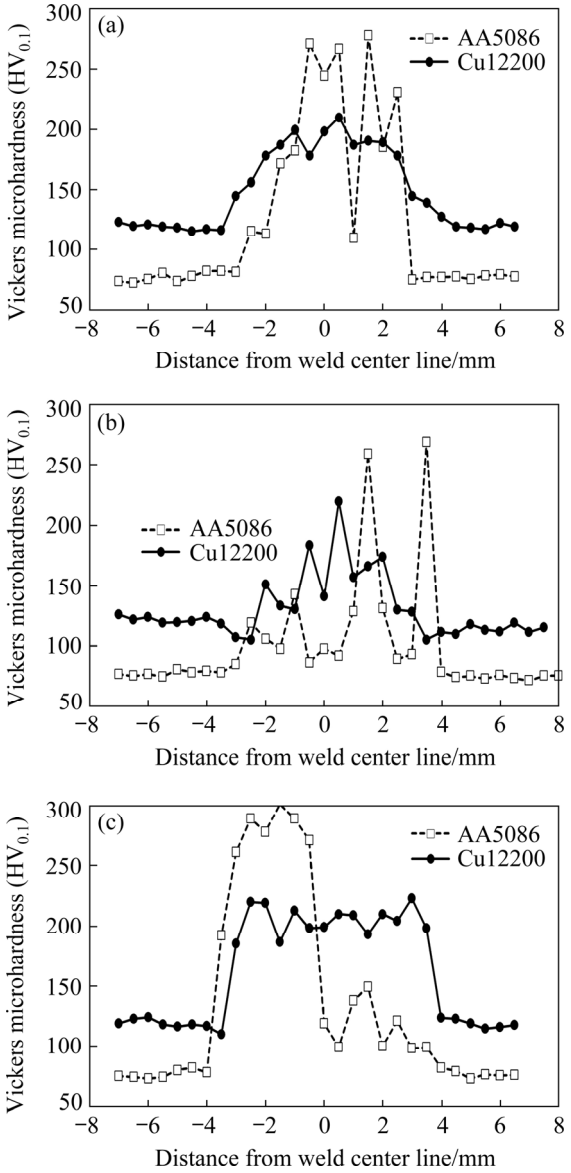

Fig. 10 Microhardness profiles of welded samples with different overlaps: (a) +0.5 mm; (b) 0 mm; (c) −0.5 mm

overlap of the second pass, the detachment of copper particles and their dispersion in the stir zone, as well as the formation of the aluminum−copper intermetallic compound, increase; thus, it can be expected that the hardness difference between the two sides of the aluminum alloy in the stir zone will increase.

It should be noted, however, that the hardness distribution in sample welded without overlap is more uniform due to the homogeneous distribution of copper particles in the aluminum matrix. Another important point is the increase in hardness in the copper layer near the weld zone in all samples. Given that the copper layer is likely to undergo the plastic deformation as well as the dynamic recrystallization, the increase in hardness can be attributed to the formation fine grains in this zone. It should be noted, however, that the magnitudes of the hardness changes in the copper layer as well as the hardness value in sample welded with on overlap of −0.5 mm, with much higher heat input, are much greater than those in other samples. The higher heat input and the higher plastic deformation in sample welded with overlap of −0.5 mm cause the copper layer to soften, resulting in severer plastic deformation in a wider area, and a larger area with hardness changes in the copper layer.

Figure 11 illustrates the ultimate tensile strength (UTS) and elongation achieved by RHTT of samples welded with different overlaps. Samples welded with overlaps of −0.5, 0, and +0.5 mm have UTS values of (311.03±2.32), (321.45±3.21), (319.42±2.56) MPa, respectively. The higher strength in sample welded without overlap may be due to its more uniform distribution of copper particles as well as more uniform hardness distribution in the stir zone.

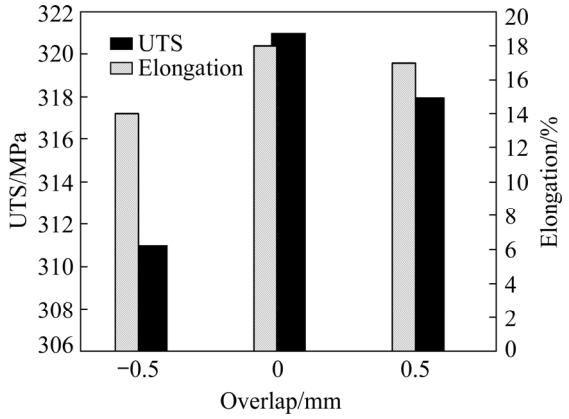

Fig. 11 Ultimate tensile strength (UTS) and elongation of welded samples with different overlaps

Due to the fact that at an overlap of 0 the best conditions in terms of hardness distribution and joint strength were achieved, the rotational speed of 600 r/min, traverse speed of 40 mm/min and overlap of 0 were used for the fabrication two-layer aluminum−copper pipe. The cross-sections of the two-layer aluminum−copper pipe are shown in two different directions in Fig. 12. As can be seen, the joint is completely integrated in both directions. X-ray diffraction (XRD) and scanning electron microscope (SEM) were used to evaluate the intermetallic constituents and microstructure formed in the welding zone, respectively.

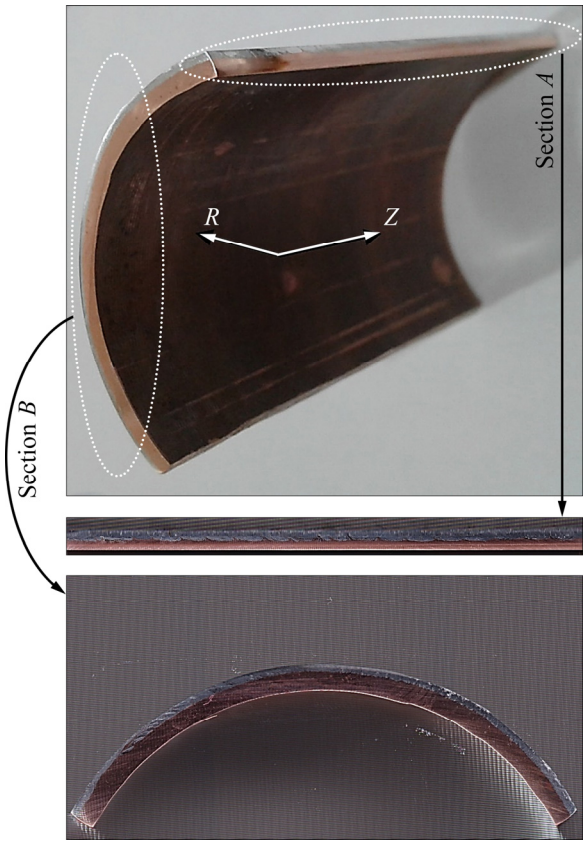

Fig. 12 Cross-sections of two-layer aluminum−copper pipe in two different directions

Figure 13 shows the SEM images of two sections in the stir zone. The thermal history associated with the plastic deformation in the friction stir welding process causes the two copper and aluminum materials in the stir zone to blend together according to their flow behavior. As shown in Fig. 13, despite the separation of parts of copper, its movement to the stir zone and the formation of separate islands of copper, the layered structure of copper in the aluminum matrix is formed in the stir zone. This phenomenon results from the simultaneous impact of heat and material flow that causes the copper metal veins to be drawn regularly from the lower part of the weld to the upper parts of the stir zone. From a metallurgical view, these layer structures are a good place to produce intermetallic.

Figure 14 shows the XRD patterns of the stir zone in two directions. Based on the X-ray diffraction results, the stir zone contains aluminum, copper, and two copper−aluminum intermetallics ($CuAl_2$ and Cu_9Al_4). The line scan analysis results are taken from the copper-rich particles present in the stir zone. The results are shown in Fig. 15.

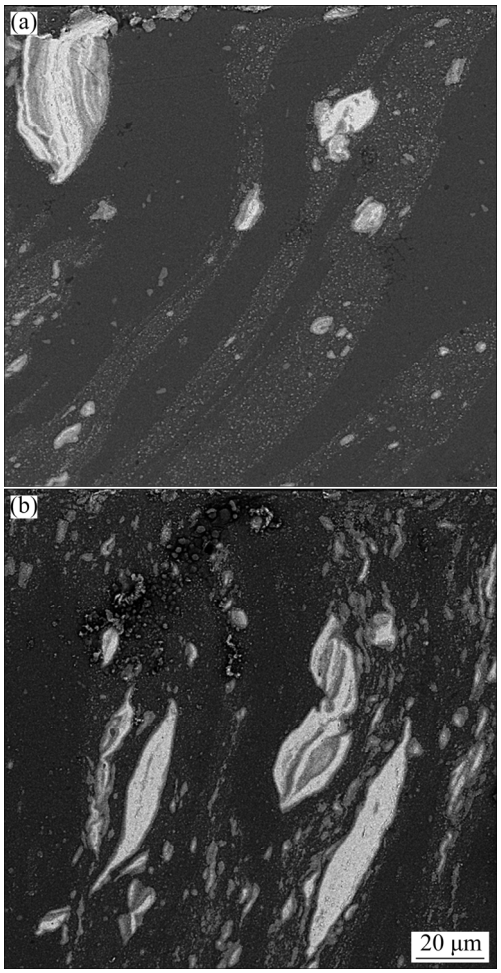

Fig. 13 SEM images of two sections in stir zone: (a) Section *A*; (b) Section *B*

As can be seen, at interface of Cu particles and Al matrix, a high density of copper and aluminum can be detected, indicating an aluminum−copper intermetallic formation in the stir zone. It should be noted that the friction stir welding process is accompanied by a severe plastic deformation of the material in the stir zone, which can greatly increase the rate of diffusion over the static state. The deformation of the material due to the rotational and traverse speeds of the tool results in the creation of thin layers of material in the stir zone. Consequently, it can be stated that due to the severe plastic deformation and temperature in the stir zone, the aluminum−copper intermetallic compounds form in the joints between the copper particles and layers.

The UTS and elongation obtained from the RHTT for two-layer pipe are (319.52±2.31) MPa and 19.47%, respectively. The fracture sample and SEM image of fracture surface are shown in Fig. 16.

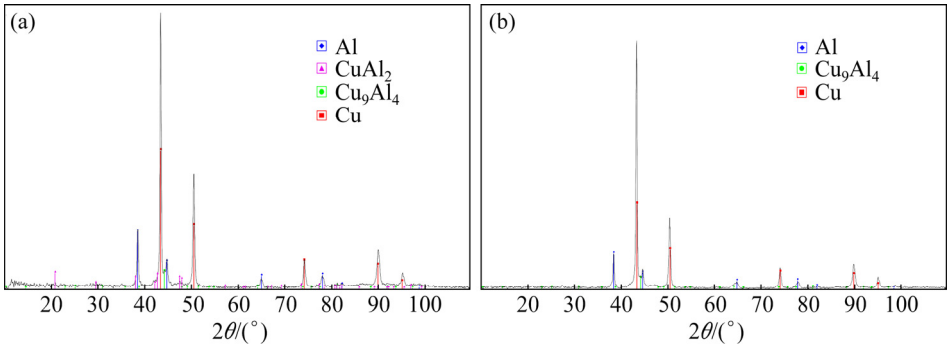

Fig. 14 XRD patterns of two sections in stir zone: (a) Section *A*; (b) Section *B*

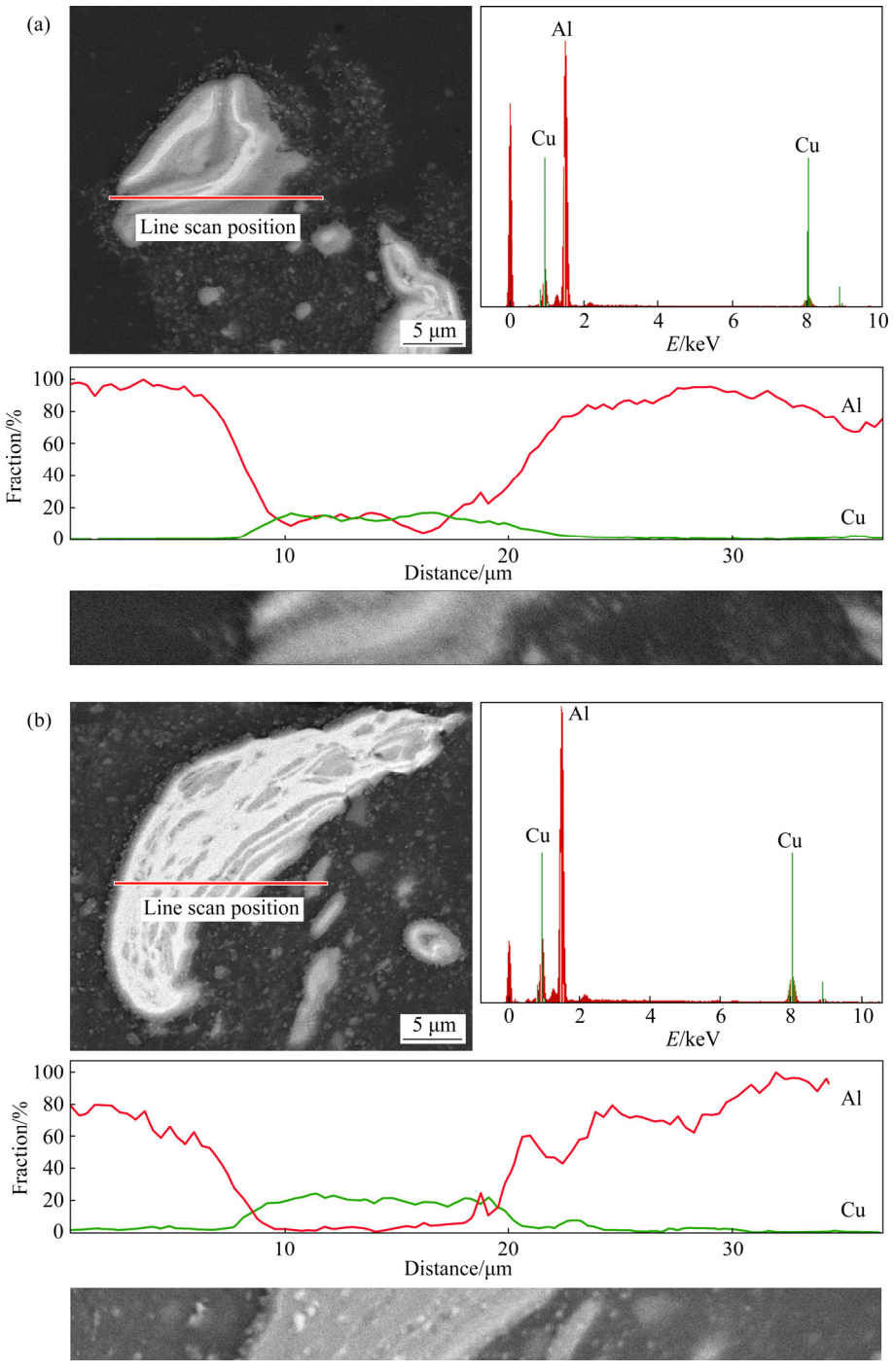

Fig. 15 Line scan analysis results of copper-rich particles in stir zone on two sections: (a) Section *A*; (b) Section *B*

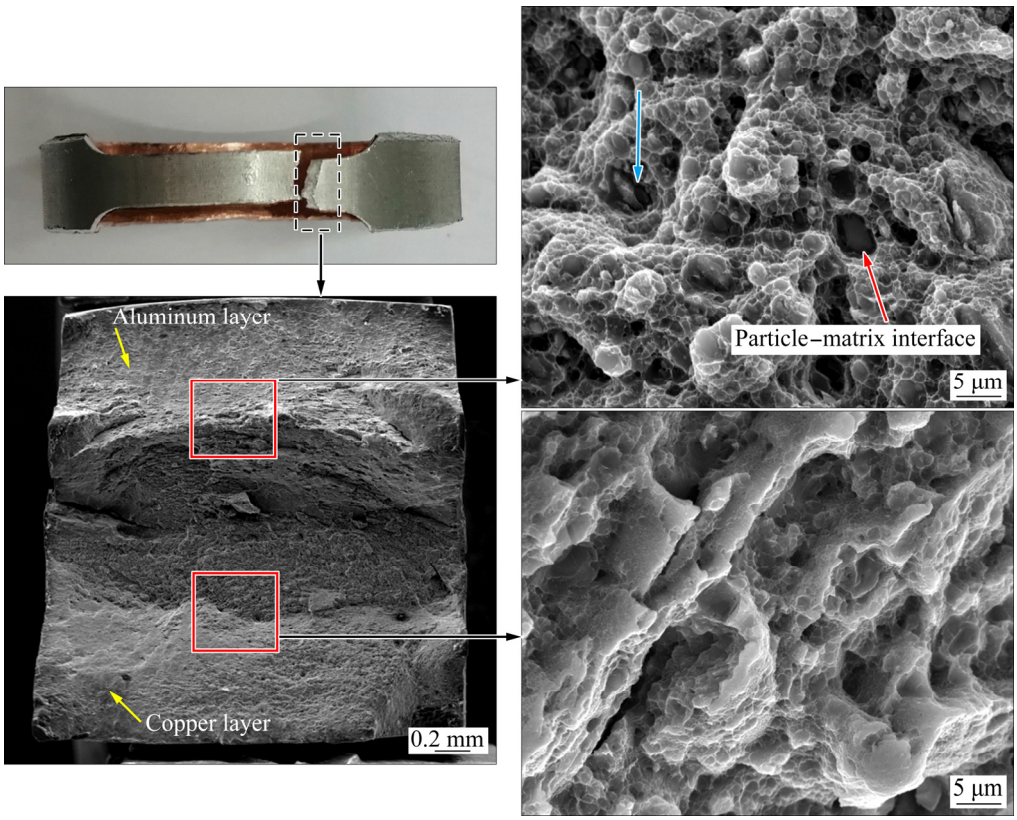

Fig. 16 Fracture sample and SEM images of fracture surface of two-layer aluminum−copper pipe

As can be seen, the separation between the layers does not occur and integrated joint in this sample can be seen. The fracture surface of the upper layer of the composite has the ductile fracture nature and also the lower layer, which does not contain copper-rich particles, exhibits ductile behavior. Another important point that can be concluded from the fracture surface of the upper layer, the bonding between the Cu-rich particles (intermetallic) and the matrix is strong so that the failure in the particles has occurred (fracture in the particles shown with a blue arrow).

5 Conclusions

(1) According to simulation results, the contribution of heat due to plastic deformation is 8% to 13% of the total heat generated during process. Also, the maximum error in estimating the maximum temperature during welding was 4.1%.

(2) The numerical models that consider the effects of strain and heat simultaneously can be effective in controlling the properties and characteristics of the weld.

(3) The temperature and strain rate profiles near the FSW tool are asymmetric, so on the advancing side, the maximum temperature and strain rate are higher than those on the retreating side.

(4) Although there is no linear trend between the ratio of rotational-to-traverse speed and the maximum temperature of the stir zone, with a good approximation, it can be stated that by decreasing this ratio the maximum temperature of stir zone increases.

(5) With increasing overlap or decreasing the overlap of passes compared to an overlap of 0, the copper particle size in the stir zone increases and the uniformity of this particle distribution is reduced. In sample welded with an overlap of 0 due to its more uniform distribution of copper particles as well as more uniform hardness distribution in the stir zone, higher joint strength is achieved.

(6) Due to the formation of equiaxed fine grains and dispersion of the aluminum−copper intermetallic in the stir zone the hardness of the stir zone on the aluminum alloy side increases compared to the aluminum base metal. The results of the hardness test show that the maximum hardness in the stir zone is in sample welded

with an overlap of −0.5 mm and equal to 301.4 $HV_{0.1}$.

(7) Due to the severe plastic deformation in the stir zone, the aluminum−copper intermetallic compounds ($CuAl_2$ and Cu_9Al_4) form in the stir zone.

(8) The fabricated two-layer pipe fractured with ductile feature and without debonding between layers. The UTS and elongation of two-layer pipe are (319.52±2.31) MPa and 19.47%, respectively.

References

[1] GIBSON I, ROSEN D, STUCKER B, KHORASANI M. Additive manufacturing technologies [M]. Boston: Springer, 2014.

[2] TARIK ARAFAT M, GIBSON I, LI X. State of the art and future direction of additive manufactured scaffolds-based bone tissue engineering [J]. Rapid Prototyping Journal, 2014, 20(1):13−26.

[3] PALANIVEL S, NELATURU P, GLASS B, MISHRA R. Friction stir additive manufacturing for high structural performance through microstructural control in an Mg based WE43 alloy [J]. Materials & Design, 2015, 65: 934−952.

[4] PALANIVEL S, SIDHAR H, MISHRA R. Friction stir additive manufacturing: Route to high structural performance [J]. JOM, 2015, 67(3): 616−621.

[5] IBRAHIM A B, AL-BADOUR F A, ADESINA A Y, MERAH N. Effect of process parameters on microstructural and mechanical properties of friction stir diffusion cladded ASTM A516-70 steel using 5052 Al alloy [J]. Journal of Manufacturing Processes, 2018, 34: 451−462.

[6] BEYGI R, KAZEMINEZHAD M, KOKABI A. Microstructural evolution and fracture behavior of friction-stir-welded Al−Cu laminated composites [J]. Metallurgical and Materials Transactions A, 2014, 45(1): 361−370.

[7] ROODGARI M R, JAMAATI R, AVAL H J. Microstructure and mechanical properties of IF/St52 steel composite produced by friction stir lap welding [J]. Materials Science and Engineering A, 2020, 772: 138775.

[8] ROODGARI M R, JAMAATI R, AVAL H J. Fabrication of a 2-layer laminated steel composite by friction stir additive manufacturing [J]. Journal of Manufacturing Processes, 2020, 51: 110−121.

[9] CHITKARA N, ALEEM A. Extrusion of axi-symmetric bi-metallic tubes: Some experiments using hollow billets and the application of a generalised slab method of analysis [J]. International Journal of Mechanical Sciences, 2001, 43(12): 2857−2882.

[10] KHOSRAVIFARD A, EBRAHIMI R. Investigation of parameters affecting interface strength in Al/Cu clad bimetal rod extrusion process [J]. Materials & Design, 2010, 31(1): 493−499.

[11] CHEN Z, IKEDA K, MURAKAMI T, TAKEDA T, XIE J X. Fabrication of composite pipes by multi-billet extrusion technique [J]. Journal of Materials Processing Technology, 2003, 137(1−3): 10−16.

[12] ACARER M, GÜLENÇ B, FINDIK F. Investigation of explosive welding parameters and their effects on microhardness and shear strength [J]. Materials & Design, 2003, 24(8): 659−664.

[13] SUN X J, JIE T, GUO X Z. Bonding properties of interface in Fe/Al clad tube prepared by explosive welding [J]. Transactions of Nonferrous Metals Society of China, 2011, 21(10): 2175−2180.

[14] BHANUMURTHY K, FOTEDAR R, JOYSON D, KALE G, PAPPACHAN A, GROVER A. Development of tubular transition joints of aluminium/stainless steel by deformation diffusion bonding [J]. Materials Science and Technology, 2006, 22(3): 321−330.

[15] ZHANG J, FAN Z Y, WANG Y Q, ZHOU B L. Hypereutectic aluminium alloy tubes with graded distribution of Mg_2Si particles prepared by centrifugal casting [J]. Materials & Design, 2000, 21(3): 149−153.

[16] MOHEBBI M, AKBARZADEH A. A novel spin-bonding process for manufacturing multilayered clad tubes [J]. Journal of Materials Processing Technology, 2010, 210(3): 510−517.

[17] WANG X S, LI P N, WANG R Z. Study on hydro-forming technology of manufacturing bimetallic CRA-lined pipe [J]. International Journal of Machine Tools and Manufacture, 2005, 45(4−5): 373−378.

[18] FAN Z S, YU H P, LI C F. Plastic deformation behavior of bi-metal tubes during magnetic pulse cladding: FE analysis and experiments [J]. Journal of Materials Processing Technology, 2016, 229: 230−243.

[19] AVAL H J, LOUREIRO A. Effect of reverse dual rotation process on properties of friction stir welding of AA7075 to AISI304 [J]. Transactions of Nonferrous Metals Society of China, 2019, 29(5): 964−975.

[20] ZHOU H, LIU J S, ZHOU D W, TAO T. Effect of Al-foil addition on microstructure and temperature field of laser fusion welded joints of DP590 dual-phase steel and AZ31B magnesium alloy [J]. Transactions of Nonferrous Metals Society of China, 2020, 30(10): 2669−2680.

[21] LIU G Q, GAO X D, CONG P, LIU X H, HUANG Y J, ZHANG Y X. Tensile resistance, microstructures of intermetallic compounds, and fracture modes of welded steel/aluminum joints produced using laser lap welding [J]. Transactions of Nonferrous Metals Society of China, 2020, 30(10): 2639−2649.

[22] EBRAHIMZADEH V, PAIDAR M, SAFARKHANIAN M, OJO O O. Orbital friction stir lap welding of AA5456-H321/AA5456-O aluminum alloys under varied parameters [J]. The International Journal of Advanced Manufacturing Technology, 2018, 96(1): 1237−1254.

[23] GERCEKCIOGLU E, EREN T, YILDIZLI K, KAHRAMAN N, SALAMCI E. Friction behaviour on the external surface of the friction stir welding of AA 6063-T6 tubes [J]. Journal of Balkan Tribological Association, 2006, 12(1): 24−29.

[24] DOOS Q M, WAHAB B A. Experimental study of friction stir welding of 6061-T6 aluminum pipe [J]. International Journal of Mechanical Engineering and Robotics Research, 2012, 1(3): 143−156.

[25] DUAN R H, XIE G M, LUO Z A, XUE P, WANG C,

MISRA R D K, WANG G D. Microstructure, crystallography, and toughness in nugget zone of friction stir welded high-strength pipeline steel [J]. Materials Science and Engineering A, 2020, 791: 139620.

[26] GIORJÃO R A R, PEREIRA V F, TERADA M, DA FONSECA E B, MARINHO R R, GARCIA D M. Microstructure and mechanical properties of friction stir welded 8 mm pipe SAF 2507 super duplex stainless steel [J]. Journal of Materials Research and Technology, 2019, 8(1): 243−249.

[27] RONEVICH J A, SOMERDAY B P, FENG Z. Hydrogen accelerated fatigue crack growth of friction stir welded X52 steel pipe [J]. International Journal of Hydrogen Energy, 2017, 42(7): 4259−4268.

[28] JAMSHIDI A H, FALAHATI N M. Orbital friction stir lap welding in tubular parts of aluminium alloy AA5083 [J]. Science and Technology of Welding and Joining, 2017, 22(7): 562−572.

[29] LI W Y, WEN Q, YANG X W, WANG Y W, GAO D, WANG W B. Interface microstructure evolution and mechanical properties of Al/Cu bimetallic tubes fabricated by a novel friction-based welding technology [J]. Materials & Design, 2017, 134: 383−393.

[30] TAVASSOLIMANESH A, ALAVI N A. A new approach for manufacturing copper−clad aluminum bimetallic tubes by friction stir welding (FSW) [J]. Journal of Manufacturing Processes, 2017, 30: 374−384.

[31] IQBAL M P, JAIN R, PAL S K. Numerical and experimental study on friction stir welding of aluminum alloy pipe [J]. Journal of Materials Processing Technology, 2019, 274: 116258.

[32] LAMMLEIN D, GIBSON B, DELAPP D, COX C, STRAUSS A, COOK G. The friction stir welding of small-diameter pipe: An experimental and numerical proof of concept for automation and manufacturing [J]. Proceedings of the Institution of Mechanical Engineers, Part B: Journal of Engineering Manufacture, 2012, 226(3): 383−398.

[33] AL-BADOUR F, MERAH N, SHUAIB A, BAZOUNE A. Coupled Eulerian Lagrangian finite element modeling of friction stir welding processes [J]. Journal of Materials Processing Technology, 2013, 213(8): 1433−1439.

[34] GAO E Z, ZHANG X X, LIU C Z. Numerical simulations on material flow behaviors in whole process of friction stir welding [J]. Transactions of Nonferrous Metals Society of China, 2018, 28(11): 2324−2334.

[35] AHLERS G. Heat capacity of copper [J]. Review of Scientific Instruments, 1966, 37(4): 477−480.

[36] KUROCHKIN A, YAGODIN D, BORISENKO A, OKHAPKIN A. Density of copper−aluminum alloys at temperatures up to 1400 °C determined by the gamma-ray technique [J]. High Temperature, 2013, 51(2): 197−205.

[37] WANG K, REEBER R R. Thermal expansion of copper [J]. High Temperature and Materials Science, 1996, 35(2): 181−186.

[38] SIDLES P H, DANIELSON G. Thermal conductivity of metals at high temperatures [R]. Technical Information Service, United States Atomic Energy Commission, 1951.

[39] AVAL H J, SERAJZADEH S, KOKABI A. Evolution of microstructures and mechanical properties in similar and dissimilar friction stir welding of AA5086 and AA6061 [J]. Materials Science and Engineering A, 2011, 528(28): 8071−8083.

[40] PRASAD Y, RAO K, SASIDHAR S. Hot working guide: A compendium of processing maps [M]. New York: ASM International, 2015.

[41] WANG H, BOUCHARD R, EAGLESON R, MARTIN P, TYSON W R. Ring hoop tension test (RHTT): A test for transverse tensile properties of tubular materials [J]. Journal of Testing and Evaluation, 2002, 30(5): 382−391.

[42] BALASUBRAMANIAN V. Relationship between base metal properties and friction stir welding process parameters [J]. Materials Science and Engineering A, 2008, 480(1−2): 397−403.

[43] AVAL H J, SERAJZADEH S, KOKABI A. The influence of tool geometry on the thermo-mechanical and microstructural behaviour in friction stir welding of AA5086 [J]. Mechanical Engineering Science, 2011, 225(1): 1−16.

[44] MIRJALILI A, SERAJZADEH S, JAMSHIDI AVAL H, KOKABI A. Modeling and experimental study on friction stir welding of artificially aged AA2017 plates [J]. Materials and Manufacturing Processes, 2013, 28(6): 683−688.

[45] HIRATA T, OGURI T, HAGINO H, TANAKA T, CHUNG S W, TAKIGAWA Y. Influence of friction stir welding parameters on grain size and formability in 5083 aluminum alloy [J]. Materials Science and Engineering A, 2007, 456(1−2): 344−349.

[46] HAMED J A. Effect of welding heat input and post-weld aging time on microstructure and mechanical properties in dissimilar friction stir welded AA7075–AA5086 [J]. Transactions of Nonferrous Metals Society of China, 2017, 27(8): 1707−1715.

[47] MORADI M M, JAMSHIDI AVAL H, JAMAATI R. Experimental investigation on the effect of friction stir welding process parameters in dissimilar joining of AA2024-T351 and AA6061-T6 aluminum alloys [J]. Modares Mechanical Engineering, 2016, 16(9): 394−402.

[48] ELANGOVAN K, BALASUBRAMANIAN V. Influences of pin profile and rotational speed of the tool on the formation of friction stir processing zone in AA2219 aluminium alloy [J]. Materials Science and Engineering A, 2007, 459(1−2): 7−18.

[49] BIKKINA V, TALASILA S R, ADEPU K. Characterization of aluminum based functionally graded composites developed via friction stir processing [J]. Transactions of Nonferrous Metals Society of China, 2020, 30(7): 1743−1755.

[50] MOAREF A, RABIEZADEH A. Microstructural evaluation and tribological properties of underwater friction stir processed CP-copper and its alloy [J]. Transactions of Nonferrous Metals Society of China, 2020, 30(4): 972−981.

[51] ASGHARZADEH A, AVAL H J, SERAJZADEH S. A study on flow behavior of AA5086 over a wide range of temperatures [J]. Journal of Materials Engineering and Performance, 2016, 25(3): 1076−1084.

[52] AWANG M. Simulation of friction stir spot welding (FSSW) process: Study of friction phenomena [D]. Morgantown: West Virginia University, 2007.

[53] NANDAN R, ROY G, DEBROY T. Numerical simulation of three-dimensional heat transfer and plastic flow during friction stir welding [J]. Metallurgical and Materials Transactions A, 2006, 37(4): 1247−1259.

[54] SHARMA N, SIDDIQUEE A N. Friction stir welding of aluminum to copper—An overview [J]. Transactions of Nonferrous Metals Society of China, 2017, 27(10): 2113−2136.

搅拌摩擦增材制造制备双层铝铜管的理论与实验研究

Mehdi FALAHATI NAQIBI[1], Majid ELYASI[1], Hamed JAMSHIDI AVAL[2], Mohammad Javad MIRNIA[1]

1. Department of Mechanical Engineering, Babol Noshirvani University of Technology, Shariati Avenue, Babol 47148-71167, Iran;
2. Department of Materials Engineering, Babol Noshirvani University of Technology, Shariati Avenue, Babol 47148-71167, Iran

摘　要：对采用搅拌摩擦增材制造(FSAM)工艺制备的双层铝铜管进行实验和数值研究。用 ABAQUS 软件建立三维热力学模型，研究制备过程中的温度和应变分布。模拟结果表明，虽然采用转动速度与移动速度比可以较好地预测焊接过程中的热输入，但是不能准确地预测焊缝截面缺陷的形成。预测结果与实验结果吻合较好，对焊接过程最高温度估计的最大误差为 4.1%。由于热和大塑性变形，搅拌区形成铝铜金属间化合物 ($CuAl_2$ 和 Cu_9Al_4)。焊接重叠区为−0.5 mm 的样品搅拌区具有最大硬度 301.4 $HV_{0.1}$。搅拌摩擦增材制造的双层管的极限抗拉强度和伸长率分别为(319.52±2.31) MPa 和 19.47%。

关键词：搅拌摩擦焊；热力学模拟；双层铝铜管；显微组织；力学性能

(Edited by Wei-ping CHEN)